Contributions to Geophysics and Geodesy Vol. 47/4, 2017 (261–276)

Magnetic and velocity fields in a dynamo operating at extremely small Ekman and magnetic Prandtl numbers

Ján ŠIMKANIN,Juraj KYSELICA

Institute of Geophysics, Czech Academy of Sciences,
Boční II/1401, 141 31 Prague, Czech Republic; e-mail: jano@ig.cas.cz, kyselica@ig.cas.cz

Abstract: Numerical simulations of the geodynamo are becoming more realistic because of advances in computer technology. Here, the geodynamo model is investigated numerically at the extremely low Ekman and magnetic Prandtl numbers using the PARODY dynamo code. These parameters are more realistic than those used in previous numerical studies of the geodynamo. Our model is based on the Boussinesq approximation and the temperature gradient between upper and lower boundaries is a source of convection. This study attempts to answer the question how realistic the geodynamo models are. Numerical results show that our dynamo belongs to the strong-field dynamos. The generated magnetic field is dipolar and large-scale while convection is small-scale and sheet-like flows (plumes) are preferred to a columnar convection. Scales of magnetic and velocity fields are separated, which enables hydromagnetic dynamos to maintain the magnetic field at the low magnetic Prandtl numbers. The inner core rotation rate is lower than that in previous geodynamo models. On the other hand, dimensional magnitudes of velocity and magnetic fields and those of the magnetic and viscous dissipation are larger than those expected in the Earth's core due to our parameter range chosen.

Key words: Hydromagnetic dynamo, Prandtl number, Magnetic Prandtl number, Inertial forces

1. Introduction

The magnetic fields of astrophysical bodies in the universe are generated by a self-consistent hydromagnetic dynamo action in the liquid parts of their interiors. The magnetic field of the Earth is also generated by a hydromagnetic dynamo that works in its outer liquid core (*Braginsky and Roberts, 1995; Roberts and Glatzmaier, 2000; Christensen and Wicht, 2007*). Observatory and satellite measurements provide us with information about the current geomagnetic field. In addition, observatory measurements are

doi: 10.1515/congeo-2017-0014

a source of information about the geomagnetic field in the past century. However, looking further into the past, archaeomagnetism and palaeomagnetism give us the only information about the geomagnetic field (*Roberts and Glatzmaier, 2000* and *Christensen and Wicht, 2007*).

Numerical modelling of the geodynamo achieved a significant development in past years, numerical models can reproduce magnetic fields that are really observed and are consistent also with knowledge provided by palaeomagnetism, e.g. they also reproduce polarity changes and excursions (*Roberts and Glatzmaier, 2000; Glatzmaier, 2005; Christensen and Wicht, 2007; Sakuraba and Roberts, 2009*). Despite this progress, many authors asked whether those models are realistic or how the results of numerical simulations describe the real observed geomagnetic field (*Roberts and Glatzmaier, 2000; Glatzmaier, 2005; Christensen and Wicht, 2007; Takahashi et al., 2008; Sakuraba and Roberts, 2009; Wicht and Tilgner, 2010; Christensen, 2011; Roberts and King, 2013*). All numerical models have been studied for parameters that did not reach parameter ranges relevant to the Earth's core. The viscosity is the first example. Geodynamo models use the values of many orders of magnitude higher than those estimated for the Earth's core. Further models use lower magnetic diffusivity than estimated in the Earth's core. Finally, the investigated models are laminar but convection in the Earth's core is turbulent. All these simplifications are forced due to computational constraints and stability of numerical schemes. Turbulent convection and low viscosity require higher spatial resolution and smaller time steps. This extends the computing time and, thus, places high demands on computing resources. In addition to parameters used in numerical modelling of geodynamo, it is necessary to mention approximations regarding the outer Earth's core. The real fluid in the Earth's core is fully compressible. For simplification, many dynamo models use the Boussinesq approximation, which assumes that the fluid is incompressible. However, this is an acceptable simplification for the Earth's core. Another step forward is the anelastic approximation, the essence of which is a compressible fluid in the limit of low Mach number. This neglects sound waves, their typical time scales are negligible compared to typical time scales of geomagnetic phenomena. Although anelastic approximation is more apppropriate, many dynamo models are still based on the Boussinesq approximation. This is mainly because it saves computing resources and the results obtained are

very similar to those provided by the anelastic approximation (*Roberts and Glatzmaier, 2000; Glatzmaier, 2005; Christensen and Wicht, 2007; Takahashi et al., 2008; Sakuraba and Roberts, 2009; Wicht and Tilgner, 2010; Christensen, 2011; Roberts and King, 2013*). Hydromagnetic flows in the Earth's core that generate the geomagnetic field are generally believed to be driven by buoyancy. The freezing of the inner core provides the thermal buoyancy from the release of latent heat at the inner core boundary (ICB), as well as compositional buoyancy as the light alloying core constituent is released during freezing. Thus, the slowly growing ICB fosters thermochemical convection, which drives the geodynamo (*Roberts and Glatzmaier, 2000; Glatzmaier, 2005; Christensen and Wicht, 2007; Takahashi et al., 2008; Sakuraba and Roberts, 2009; Wicht and Tilgner, 2010; Christensen, 2011; Roberts and King, 2013; Kyselica and Guba, 2016; Šimkanin et al., 2017*). Thus, superadiabatic radial temperature, concentration or thermochemical gradients between the ICB and the core-mantle boundary (CMB) are the source of buoyancy in many geodynamo models. Further models contain internal heat sources, which allow studying the density stratified spherical shells also in the Boussinesq approximation. The precessionally driven hydromagnetic dynamos are possible, too. Previously, it was assumed that a dynamo could not be precessionally or tidally driven, however, those models were linear. Thus, the kinetic energy of fluid motions strongly dissipated in the boundary layers, leading to malfunctioning dynamo. However, reflecting non-linear terms (the full 3D dynamo problem), numerical simulations showed that precessionally driven dynamos do exist and can provide dipolar magnetic fields. Similarly, it appears that the tidally driven flows do not markedly dissipate in the boundary layers. Thus, precessionally and tidally driven flows can be a source for a hydromagnetic dynamo (*Le Bars et al., 2011*). The current state of numerical dynamo modelling is described very well by *Christensen and Wicht (2007), Takahashi et al. (2008), Sakuraba and Roberts (2009), Wicht and Tilgner (2010), Christensen (2011), Takahashi and Shimizu (2012), Roberts and King (2013).*

Since the first 3D self-consistent dynamo simulation performed by Glatzmaier and Roberts, numerical modelling of self-consistent dynamos made huge progress but the models studied later used larger values of viscosity than those used by *Roberts and Glatzmaier (2000).* Nevertheless, these were able to clarify many of the physical mechanisms that accompany the

geomagnetic field generation. *Sakuraba and Roberts (2009)* and *Soderlund et al. (2015)* used lower values of viscosity than those used by *Roberts and Glatzmaier (2000)*, however, their models were different. *Sakuraba and Roberts (2009)* investigated how the results from two otherwise identical models differed when the temperature of the CMB was specified in two distinct ways. Their Uniform Surface Temperature Model (USTM) used the same thermal conditions as those used by *Soderlund et al. (2015)*. Their Uniform Heat Flux Model (UHFM) assumed the same total heat emerged from the core, but achieved that by prescribing constant radial temperature gradient. Their results showed that UHFM created a strong Earth-like field and large-scale magnetic field and flow patterns were a robust characteristic for smaller viscosities. A difference between USTM and UHFM laid in different ability to create large-scale circulation in the core. Another parameters that limit numerical simulations are the diffusivities. For the Earth's outer core the kinematic viscosity $\nu = 10^{-6}\,\mathrm{m^2\,s^{-1}}$, the thermal diffusivity $\kappa = 5 \times 10^{-6}\,\mathrm{m^2\,s^{-1}}$ and the magnetic diffusivity $\eta = 2\,\mathrm{m^2\,s^{-1}}$ are typical estimates (*Fearn, 2007; Roberts and Glatzmaier, 2000*). In most numerical simulations scientists set $\nu/\kappa = 1$ (the ratio ν/κ is known as the Prandtl number). *Christensen and Wicht (2007)* estimated that values of ν/κ for the Earth's outer core lie between 0.1 and 1. Recent estimates of the thermal diffusivity suggest that the values of κ range from $\kappa = 1.4 \times 10^{-7}\,\mathrm{m^2\,s^{-1}}$ to $\kappa = 9.3 \times 10^{-6}\,\mathrm{m^2\,s^{-1}}$ and lead to acceptance of ν/κ from interval $0.1 - 7$, which is consistent with the values expected for thermally driven dynamos ($\nu/\kappa < 1$) and for thermochemically driven ones ($\nu/\kappa > 1$). Original estimates for the magnetic diffusivity, η, suggested $\eta = 2\,\mathrm{m^2\,s^{-1}}$, which resulted in $\nu/\eta = 10^{-6}$ (the ratio ν/η is known as the magnetic Prandtl number, P_m). However, some recent estimates give values of η that are much larger, $\eta = 12\,\mathrm{m^2\,s^{-1}}$, which leads to a larger value of the magnetic Prandtl number, $\nu/\eta = 10^{-5}$. Recent estimates of the thermal and magnetic diffusivities have been done by *Pozzo et al. (2012)* and *Gomi et al. (2013)*.

To investigate the generated magnetic fields at the lower values of viscosity, the Prandtl and magnetic Prandtl numbers than those used in the previous models is the prime motivation of the present study. We take approximately the same value of viscosity as used by *Sakuraba and Roberts (2009)* but our values of the Prandtl and magnetic Prandtl numbers are lower. The model and governing equations are presented in Section 2, nu-

merical results are provided in Section 3 and Section 4 is devoted to the discussion of the results and to conclusions.

2. Model and basic equations

Here we consider dynamo action that is due to thermal convection of an electrically conducting incompressible fluid in the Boussinesq approximation, in a spherical shell ($r_i < r < r_o$) rotating with angular velocity Ω. The evolution of the magnetic field $\mathbf{B}$, the velocity $\mathbf{V}$ and the temperature T are described by the following system of dimensionless equations:

$$E\left(\frac{\partial \mathbf{V}}{\partial t} + (\mathbf{V}\cdot\nabla)\,\mathbf{V} - \nabla^2\mathbf{V}\right) + 2\mathbf{1}_z \times \mathbf{V} + \nabla P = \\ = R_a \frac{\mathbf{r}}{r_o} T + \frac{1}{P_m}(\nabla \times \mathbf{B}) \times \mathbf{B}\,, \tag{1}$$

$$\frac{\partial \mathbf{B}}{\partial t} = \nabla \times (\mathbf{V} \times \mathbf{B}) + \frac{1}{P_m}\nabla^2\mathbf{B}\,, \tag{2}$$

$$\frac{\partial T}{\partial t} + (\mathbf{V}\cdot\nabla)\,T = \frac{1}{P_r}\nabla^2 T\,, \tag{3}$$

$$\nabla\cdot\mathbf{V} = 0\,, \qquad \nabla\cdot\mathbf{B} = 0\,. \tag{4}$$

The shell gap $L = r_o - r_i$ is used as the typical length. The aspect ratio of the inner core, r_i/r_o , is set to 0.35, which is the current value for the Earth. $(r,\, \theta,\, \varphi)$ is the spherical system of coordinates, $\mathbf{1}_z$ is the unit vector. Time, t, is measured in the unit of L^2/ν, velocity, $\mathbf{V}$, in ν/L, magnetic induction, $\mathbf{B}$, in $(\rho\mu\eta\Omega)^{1/2}$, temperature, T, in ΔT, and pressure, P, in $\rho\nu^2/L^2$. The dimensionless parameters appearing in Eqs. (1)-(4) are the Prandtl number, $P_r = \nu/\kappa$, the magnetic Prandtl number, $P_m = \nu/\eta$, the Ekman number, $E = \nu/\Omega L^2$ and the modified Rayleigh number $R_a = \alpha g_0 \Delta T L/\nu\Omega$; in the above expressions κ is the thermal diffusivity, ν is the kinematic viscosity, μ is the magnetic permeability, η is the magnetic diffusivity, ρ is the density, α is the coefficient of thermal expansion, ΔT is the drop of temperature through the shell and g_0 is the gravity acceleration at $r = r_o$.

Eqs. (1)-(4) are closed by the non-penetrating and no-slip boundary conditions for the velocity field at the rigid surfaces and those of fixed temperature boundary conditions (the constant temperature $T_i = 1$ and $T_o = 0$ at

the inner and outer boundaries of the shell, respectively). The outer boundary is electrically insulating (the magnetic field on this boundary matches with the appropriate potential field in the exterior which implies no external sources of the field), while the inner boundary is electrically conducting (electric conductivities of the outer and inner core are assumed to be the same, and B is continuous across $r = r_i$).

3. Results

Eqs. (1)-(4) are solved using the PARODY dynamo code (*Dormy, 1997; Dormy et al., 1998; Aubert et al., 2008; Raynaud and Dormy, 2013*). The PARODY code solves the non-dimensional Boussinesq equations for time-dependent thermal convection in a rotating spherical shell filled with an electrically conducting fluid. It is a semi-spectral method, using spherical-harmonics decomposition in the θ- and φ-directions, and second-order finite differencing in the r-direction. This makes it suitable for parallel computation on distributed memory clusters. Parallelization is carried out using the message-passing interface (MPI). The time integration uses the implicit second-order Crank-Nicolson scheme (*Dormy, 1997; Dormy et al., 1998; Aubert et al., 2008; Raynaud and Dormy, 2013*). To present our results, the MATLAB routines provided by Julien Aubert are used for the visualization (*Aubert et al., 2008*). The computations were performed in the Jülich Supercomputing Centre on the Supercomputer JUROPA and the visualizations on the NEMO cluster (SGI) at the Institute of Geophysics, the Czech Academy of Sciences, Prague.

In our simulation, the spatial resolution was set to $(N_r \times N_\theta \times N_\varphi) = (2304 \times 1152 \times 2304)$, where N_r, N_θ, N_φ are the numbers of grid points in the r-, θ-, φ-directions. Computations started from zero initial velocity and a strong dipole-dominated field with $B \sim \mathcal{O}(1)$. The control parameters are E, P_r, P_m, and R_a and are summarised in Table 1, which also shows corresponding values for the Earth's core and for the similar model of *Sakuraba and Roberts (2009)*. Our magnetic Prandtl number is much smaller than that of *Sakuraba and Roberts (2009)*, as well as our Prandtl number, which is more earth-like. Our Rayleigh number exceeds the critical Rayleigh number, $R_{a,c}$, for which convection is marginally possible, by

a factor of 3.23. However, our R_a is smaller than the one used by *Sakuraba and Roberts (2009)*. Therefore, their convection is more overcritical than ours. At $P_r = 0.2$, thermal diffusion processes dominate over the viscous ones because the characteristic viscous diffusion time is five times greater than the characteristic thermal diffusion time.

Table 1. Control parameters used in our simulation, in dynamo simulations of *Sakuraba and Roberts, 2009*, and the typical values for the Earth's core.

Parameter	Our model	Sakuraba & Roberts 2009	Earth's core
E	10^{-7}	1.2×10^{-7}	10^{-15}
P_r	0.2	1	0.2
P_m	9×10^{-3}	0.2	5×10^{-6}
R_a	1.5×10^5	9×10^9	10^{24}

At $E = 10^{-7}$, $P_{m_{min}} \simeq 2.5 \times 10^{-3}$, where $P_{m_{min}}$ is the minimum value of the magnetic Prandtl number, at which dipolar dynamos exist. *Christensen and Aubert (2006)* showed that this value varies with the Ekman number as

$$P_{m_{min}} \simeq 450 E^{3/4} . \tag{5}$$

This empirical relation was confirmed for $P_r = 1$ and $E \geq 3 \times 10^{-6}$ (*Christensen and Aubert, 2006; Takahashi and Shimizu, 2012*).

The output parameters are provided in Table 2. They are presented in both the dimensionless (as they have been computed) and the dimensional forms (to point out how realistic they are). Results show that the dimensionless magnetic energy, E_m, is approximately 50 times greater than the dimensionless kinetic energy of the outer core, E_k. In its dimensional form, E_m is much greater than E_k. The Elsasser number, Λ, is greater than one, which is a feature typical for the strong-field dynamos. The magnetic Reynold number, R_m, is large enough to maintain a working hydromagnetic dynamo. The Rossby number, R_o, is small so that the effects of inertia are not observable as it was the case by *Šimkanin and Hejda (2011, 2013)*. A similar situation occured at $E = 10^{-6}$ in the study by *Šimkanin (2016)*, although our $P_m \sim P_{m_{min}}$. It should be noted that the effects of the inertia can be neglected mostly when $P_m > P_{m_{min}}$ as was shown in *Šimkanin and Hejda (2011, 2013)* and *Šimkanin (2016)*.

We now focus on the power and angular momentum balances. Power supply, PB, represents the buoyant power input that maintains the dynamo.

Table 2. Output parameters.

Name of entry	Symbol	Dimensionless value	Dimensional value	Unit
Kinetic Energy (outer core)	E_k	8.7×10^7	3.5×10^{21}	J
Magnetic Energy (outer+ inner core)	E_m	2.6×10^9	1.88×10^{32}	J
Fluid Velocity	V	5.06×10^4	0.83	$\mathrm{m\,s^{-1}}$
Magnetic Field	B	8.47	0.013	T
Rossby number	R_o	1.32×10^{-3}		
Magnetic Reynolds number	R_m	119		
Elsasser number	Λ	4.68		
Power supply	PB	1.45×10^{14}	3.59×10^{16}	W
Viscous dissipation	Q_ν	1.8×10^{13}	4.45×10^{15}	W
Ohmic dissipation	Q_η	1.27×10^{14}	3.14×10^{16}	W
Viscous torque	Γ_ν	7.3×10^{13}	3.47×10^{27}	$\mathrm{kg\,m^2\,s^{-1}}$
Magnetic torque	Γ_η	-4.13×10^8	-3.47×10^{27}	$\mathrm{kg\,m^2\,s^{-1}}$
Inner core rotation rate	ω_i	5.4×10^3	3.94×10^{-8}	°/s

PB has to be balanced by the viscous dissipation, Q_ν, and the ohmic dissipation, Q_η. As provided in Table 2, $Q_\eta/Q_\nu = \mathcal{O}(10)$ and that $Q_\eta + Q_\nu$ is balanced with PB, which shows our solution has got to its approximately steady state. The angular momentum balance is given by the angular momentum equation, which in the dimensional form, takes the following form:

$$I\frac{\mathrm{d}\omega_i}{\mathrm{d}t} = \Gamma_\eta + \Gamma_\nu, \tag{6}$$

where I is the moment of inertia of the inner core, ω_i is the inner core rotation rate, Γ_η is the magnetic torque and Γ_ν is the viscous torque. The inner core is free to move, which leads to the so-called superrotation (for more details, see *Roberts and Glatzmaier, 2000*). In our case, $\omega_i = 3.94 \times 10^{-8}$ °/s, which gives 1.2 °/year, see Table 2.

The typical spatial distribution (Hammer projection) of radial magnetic field component, B_r, at $r = r_o$ is depicted in Fig. 1, as well as the equatorial sections of the radial components of the magnetic and velocity fields, B_r and V_r, respectively, and the temperature field. All the panels are snapshots taken at the time $t = 2$. The red (blue) colours indicate positive (negative) values. The generated magnetic field is dipolar with large-scale structure (see Figs 1 and 3). However, small-scale structures are more visible com-

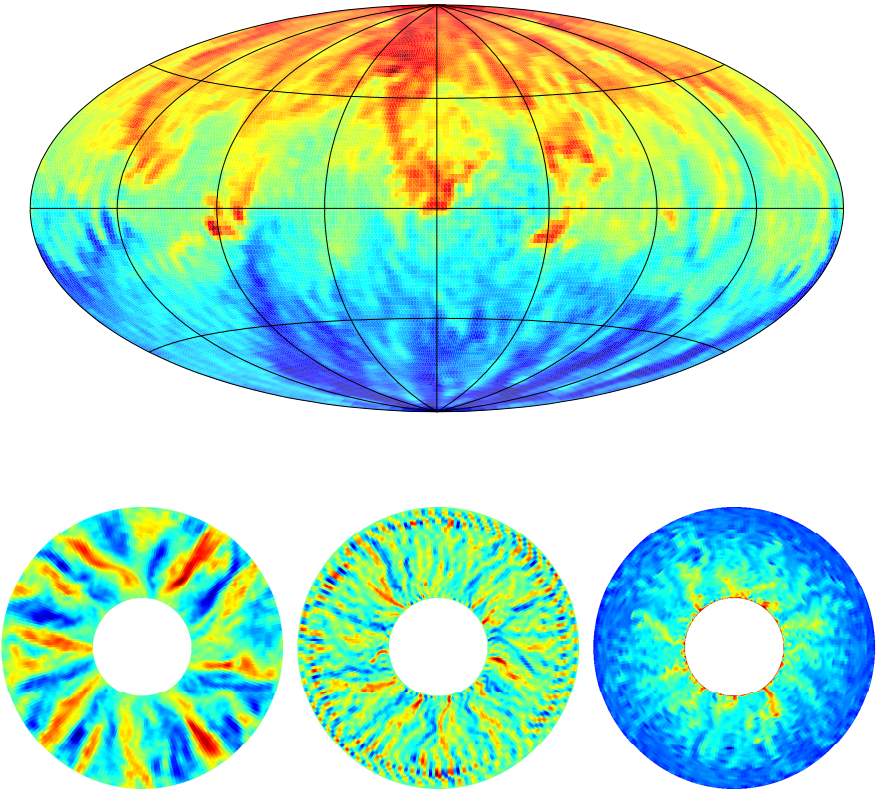

Fig. 1. Spatial distribution (Hammer projection) of radial magnetic field component, B_r, at $r = r_o$ (the top row) and equatorial sections of the radial components of the magnetic field, $\mathbf{B}$, the velocity field, $\mathbf{V}$, and the temperature, T (the bottom row), for the Rayleigh number $R_a = 1.5 \times 10^5$, the Ekman number $E = 10^{-7}$, the Prandtl number $P_r = 0.2$ and the magnetic Prandtl number $P_m = 9 \times 10^{-3}$. Red (blue) colours indicate positive (negative) values. The snapshots correspond to $t = 2$.

pared to the situation with larger values of E. A large-scale structure of the magnetic field is also visible on the equatorial section of B_r while the velocity field is small-scale. Having compared our magnetic field with those in Fig. 1 of *Sakuraba and Roberts (2009)*, we found that our results are very similar to the USTM model presented in their analysis. Similarly as for the USTM model, large-scale flux patches are not apparent in the present case. The small-scale character of convection is a result of the small value of the

Ekman number. As seen in Fig. 1, the convection has the form of sheet-like flows (or sheet plumes). This supports the results provided in *Takahashi and Shimizu (2012)* and *Kageyama et al. (2008)*. They showed that at the small Ekman number the convection has the form of sheet plumes or radial sheet jets rather than the columnar convection as the typical feature at the large Ekman numbers. This character does not depend on boundary conditions and driving mode of convection (*Takahashi and Shimizu, 2012; Kageyama et al., 2008*). The temperature distribution, shown in Fig. 1, is not as typical as for a columnar convection, instead of that, thermal plumes are observed.

Meridional sections of the poloidal and toroidal magnetic field components, B_P and B_T, respectively, as well as the poloidal and toroidal velocity field components, V_P and V_T, respectively, are presented in Fig. 2. All the panels are snapshots taken at $t = 2$. Similarly as in the study by *Šimkanin (2016)*, where $E = 10^{-6}$ was used, the magnetic field is regenerated in the tangent cylinder. It is not a surprising fact since the value of R_o is small in the present case. Thus, the magnetic field is strong enough to initiate the effect described by *Sreenivasan and Jones (2006)*. *Šimkanin and Hejda (2011, 2013)* showed that the absence of this effect is responsible for the weak magnetic field in the polar regions at low Prandtl numbers and at $P_m \sim P_{m_{\min}}$. In their studies, the magnetic field was not regenerated in the tangent cylinder, which led to the magnetic field being weak in the polar regions. The present study shows that at low E the magnetic field is regenerated in the tangent cylinder despite the fact that our P_r is low and $P_m \sim P_{m_{\min}}$. Inside the tangent cylinder, in the region of the polar vortices, thermal winds are strongly modified by magnetic winds due to Lorentz force. Therefore, the magnetic field is strong enough to initiate the polar magnetic upwelling, which stabilises the stronger magnetic field in the polar region. Consequently, we conclude that the weak magnetic field in the polar region, as a consequence of the absence of the effect described in *Sreenivasan and Jones (2006)* and *Šimkanin and Hejda (2011, 2013)*, is observable mainly at larger values of the Ekman number while at low Ekman numbers this phenomenon does not occur. The results of *Šimkanin (2016)*, together with the results presented in the present paper, support this conclusion and show that the Lorentz and Coriolis forces dominate the viscous one and the inertia.

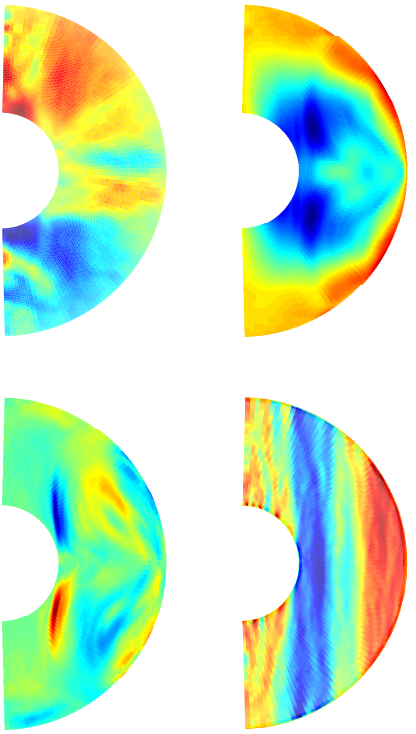

Fig. 2. Meridional sections of the poloidal and toroidal magnetic field components, B_P and B_T, respectively (top row, from left to right), and the meridional sections of the poloidal and toroidal velocity field components, V_P and V_T, respectively (bottom row, from left to right). Values of the dimensionless parapeters are $R_a = 1.5 \times 10^5$, $E = 10^{-7}$, $P_r = 0.2$ and $P_m = 9 \times 10^{-3}$. Red (blue) colours indicate positive (negative) values. The snapshots correspond to $t = 2$.

The separation of scales of the magnetic and velocity fields is clearly visible in Fig. 3, where we show the spectra of the mean-square magnetic and velocity field powers. The generated magnetic field is dominated by a large-scale axial dipole field but for the velocity field higher harmonics dominate (the velocity field has the form of small-scale sheet plumes). The scale separation enables hydromagnetic dynamos to maintain the magnetic field at low values of P_m (for more details, see *Takahashi and Shimizu, 2012*). The scale separation also explains why $P_{m_{\min}}$ decreases with decrease of E (*Takahashi and Shimizu, 2012; Christensen and Aubert, 2006*).

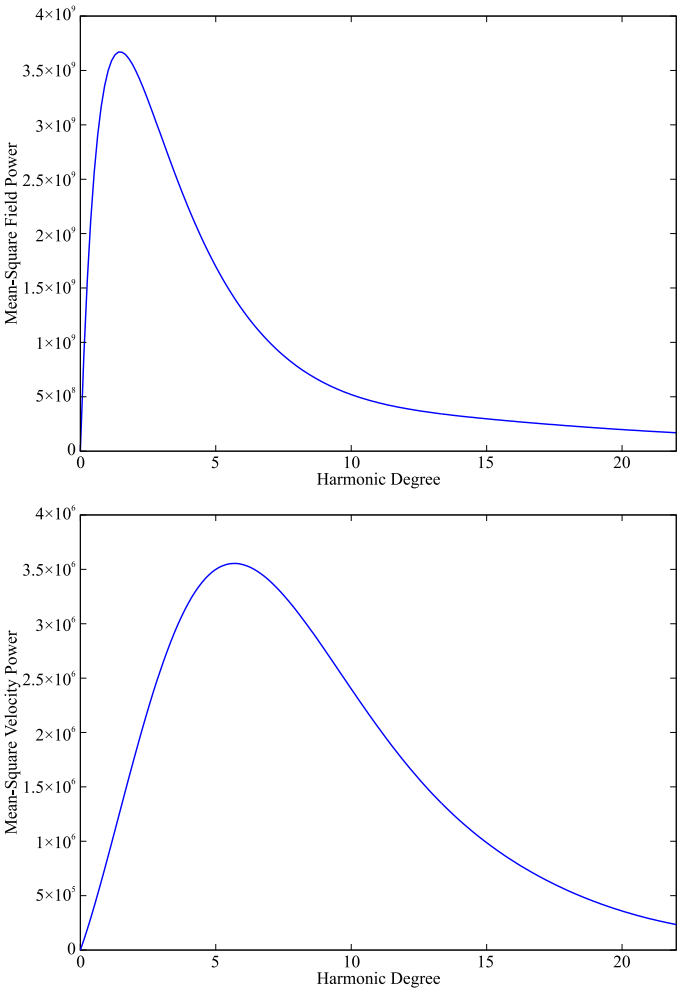

Fig. 3. The mean-square magnetic field power spectrum (top) and the mean-square velocity field power spectrum (bottom) as functions of harmonic degree l.

4. Conclusions

In this study, hydromagnetic dynamos are investigated at extremely small values of Ekman and magnetic Prandtl numbers, which we believe to be a step to a more realistic geodynamo model. *Roberts and Glatzmaier (2000),*

Glatzmaier (2005), Roberts and King (2013) posed a question whether dynamo models are realistic and how realistic they are. Now we look at our extremely small parameters to see how realistic they are. Setting $\Omega = 7.29 \times 10^{-5}\,\mathrm{rad\,s^{-1}}$ and $L = 2.26 \times 10^{6}\,\mathrm{m}$ (as given for the Earth), we obtain in dimensional forms:

- $E = 10^{-7} \quad \Rightarrow \quad \nu = 35.19\,\mathrm{m^2\,s^{-1}}$
- $P_m = 9 \times 10^{-3} \quad \Rightarrow \quad \eta = 4.13 \times 10^{3}\,\mathrm{m^2\,s^{-1}}$
- $P_r = 0.2 \quad \Rightarrow \quad \kappa = 185.98\,\mathrm{m^2\,s^{-1}}$

Most estimates of the viscosity are $\nu = 10^{-6}\mathrm{m^2\,s^{-1}}$, which makes $E = 10^{-15}$. We use "extremely low" $E = 10^{-7}$, which gives $\nu = 35.19\,\mathrm{m^2\,s^{-1}}$. This viscosity is much larger than that of any liquid readily available. Another small parameter that limits numerical simulation is P_m. Most estimates of the magnetic diffusivity are $\eta = 2\,\mathrm{m^2\,s^{-1}}$, which gives for the Earth's core $P_m = 10^{-6}$ but our small $P_m = 9 \times 10^{-3}$ and $\nu = 35.19\,\mathrm{m^2\,s^{-1}}$ gives $\eta = 4.13 \times 10^{3}\mathrm{m^2\,s^{-1}}$. Using $P_r = 0.2$ and taking $\nu = 35.19\mathrm{m^2\,s^{-1}}$ we obtain $\kappa = 185.98\,\mathrm{m^2\,s^{-1}}$ instead of $\kappa = 5 \times 10^{-6}\,\mathrm{m^2\,s^{-1}}$, which would be as exptected for the Earth's core. Consequently, we still cannot reach parameter ranges relevant to the Earth's core. Another parameter that is impossible to reach computationally is R_a. We use $R_a = 3.23R_{a,c}$, which represents the laminar convection. However, the convection in the Earth's core is turbulent, i.e. high developed ($R_a \gg R_{a,c}$). Thus, in terms of the control parameters, our dynamo model is still out of ranges relevant to the Earth's core. In addition, the model utilises the Boussinesq approximation (the incompressible fluid) instead of a fully compressible fluid of the Earth's core. The anelastic approximation seems to be more realistic than the Boussinesq one. Our dynamo is driven by the temperature gradient between the CMB and the ICB, instead of more realistic heat flux from the ICB due to solidification processes in the inner Earth's core. Therefore, though more realistic than the previous models, the present model is still not a real geodynamo.

The mean square root velocity in the present case is $V = 0.83\,\mathrm{m\,s^{-1}}$, which is much larger than the typical fluid velocity in the Earth's core, $V_E = 4 \times 10^{-4}\,\mathrm{m\,s^{-1}}$. The mean square root magnetic field is $B = 0.013\,\mathrm{T}$, which is a field that is stronger than the typical Earth's magnetic field strength 3×10^{-3} T. In addition, we assume $P_m \sim P_{m_{\min}}$ while for the Earth's core it should be $P_m > P_{m_{\min}}$ (in case the empirical relation (5)

is valid at $E = 10^{-15}$). Values of E_m and Λ show that our dynamo is the strong-field dynamo, which is expected for the real geodynamo. This implies that our solution bifurcated from the bifurcation point $R_{a,c}$ to the strong-field branch (see Fig. 19 by *Roberts and King, 2013*). It should be noted that the most of geodynamo models are α^2 – weak field dynamos instead of the $\alpha\omega$ – strong field dynamos, which is expected for the real geodynamo in the Earth's core (*Christensen and Wicht, 2007* and *Roberts and King, 2013*).

Our inner core rotation rate $\omega_i = 1.2\,^\circ$/year, which is more realistic than 2–3 $^\circ$/year, as provided in previous numerical simulations (*Christensen and Wicht, 2007* and *Roberts and King, 2013*). For the Earth's core, 0.25–0.48 $^\circ$/year is expected. Our results support the conclusion of *Roberts and Glatzmaier (2000)*, who showed that the large value of ω_i is due to E being too large than expected for the Earth's core (as usual in numerical simulations, ours included). For the Earth's core, the values of the magnetic and the viscous torques are unknown. Thus, we are not able to compare them with our results.

Our buoyant power input, viscous and ohmic dissipations are roughly 10^{16} W. However, the estimate for the Earth's core is roughly 1 TW, so our results give 10^4-times enhanced values. An explanation should follow from our parameter range. Values of velocity and magnetic field are enhanced, in comparison with the Earth's parameter regime, so that the dissipation is expected to be enhanced as well, particularly at $P_m \sim P_{m_{\min}}$.

In Table 2 we see that the inertia, characterised by the Rossby number, R_o, is low and does not affect the dynamo action. This supports the results provided by *Šimkanin (2016)* and in particular by *Soderlund et al. (2015)*, where the authors showed that at low E the inertia is negligible.

Finally, one could argue that our computations were performed only for two time units. However, despite the relatively short time interval considered, our solution almost reached its steady state. Moreover, we had to take into account the limitation for the CPU time. Forasmuch as we had to use high spatial resolution, which led to very small time step, so that the computation were too costly and CPU time consuming. Even though we have used extremely low values of the Ekman and magnetic Prandtl numbers, it would be necessary to use even lower values of E and P_m and higher values of R_a (turbulent dynamo models) in order to reach the parametric regime

of the Earth. In addition, it would be necessary to utilise rather anelastic models, which would be driven by the heat flux from the ICB.

Acknowledgements. This research has been supported by the Ministry of Education, Youth and Sports through project No. LG13042 and the Jülich Supercomputing Centre through project No. 99000539. We would like to thank Emmanuel Dormy and Julien Aubert for the PARODY dynamo code and the DMFI visualization tools, the Jülich Supercomputing Centre for CPU time on the Supercomputer JUROPA and the Institute of Geophysics, Czech Academy of Sciences, Prague for CPU time on the NEMO cluster (SGI).

References

Aubert J., Aurnou J., Wicht J., 2008: The magnetic structure of convection-driven numerical dynamos. Geophys. J. Int., **172**, 945–956.

Braginsky S. I., Roberts P. H., 1995: Equations governing convection in the Earth's core and the geodynamo. Geophys. Astrophys. Fluid Dynam., **79**, 1-4, 1–97.

Christensen U. R., Aubert J., 2006: Scaling properties of convection-driven dynamos in rotating spherical shells and application to planetary magnetic fields. Geophys. J. Int., **166**, 97–114.

Christensen U. R., Wicht J., 2007: Numerical dynamo simulations. In: Kono M. (Ed.), Volume **8** – Core Dynamics, 245–282, Schubert G. (Ed.-in-Chief), Treatise on Geophysics, Elsevier, Amsterdam, The Netherlands.

Christensen U. R., 2011: Geodynamo models: Tools for understanding properties of Earth's magnetic field. Phys. Earth Planet. Int., **187**, 157–169.

Dormy E., 1997: Numerical modeling of the geodynamo (Modélisation numérique de la dynamo terrestre). PhD thesis, Institut de Physique du Globe de Paris (in French).

Dormy E., Cardin P., Jault D., 1998: MHD flow in a slightly differentially rotating spherical shell, with conducting inner core, in a dipolar magnetic field. Earth Planet. Sci. Lett., **160**, 1-2, 15-30.

Fearn D. R., 2007: 4.1. The Earth and its magnetic field, In: Soward A. M., Dormy E. (Eds.), Mathematical Aspects of Natural Dynamos, 201–209, CRC Press, New York, USA.

Glatzmaier G. A., 2005: Planetary and stellar dynamos: challenges for next generation models, In: Soward A. M., Jones C. A., Hughes D. W., Weiss N. O. (Eds.), Fluid Dynamics and Dynamos in Astrophysics and Geophysics, 331–357, CRC Press, New York, USA.

Gomi H., Ohta K., Hirose K., Labrosse S., Caracas R., Verstraete M. J., Hernlund J. W., 2013: The high conductivity of iron and thermal evolution of the Earth's core. Phys. Earth Planet. Inter., **224**, 88–103.

Kageyama A., Miyagoshi T., Sato T., 2008: Formulation of current coils in geodynamo simulations. Nature, **454**, 1106–1109.

Kyselica J., Guba P., 2016: Forced flow and solidification over a moving substrate. Appl. Math. Model., **40**, 31–40.

Le Bars M., Wieczrorek M. A., Karatekin Ö., Cébron D., Laneuville M., 2011: An impact-driven dynamo for the early Moon. Nature, **479**, 215–218, doi: 10.1038/nature 10565.

Pozzo M., Davies C., Gubbins D., Alfè D., 2012: Thermal and electrical conductivity of iron at Earth's core conditions. Nature, **485**, 355–358, doi: 10.1038/nature 11031.

Raynaud R., Dormy E., 2013: Intermittency in spherical Couette dynamos. Phys. Rev. E, **87**, 033011.

Roberts P. H., Glatzmaier G. A., 2000: Geodynamo theory and simulations. Rev. Mod. Phys., **72**, 4, 1081–1123.

Roberts P. H., King E. M., 2013: On the genesis of the Earth's magnetism. Rep. Prog. Phys., **76**, 096801–096856.

Sakuraba A., Roberts P. H., 2009: Generation of a strong magnetic field using uniform heat flux at the surface of the core. Nature Geosci., **2**, 802–805.

Šimkanin J., Hejda P., 2011: Hydromagnetic dynamos in rotating spherical fluid shells in dependence on the Prandtl number and stratification. Geophys. J. Int., **185**, 637–646.

Šimkanin J., Hejda P., 2013: Magnetic fields generated by hydromagnetic dynamos at the low Prandtl number in dependence on the Ekman and magnetic Prandtl numbers. Phys. Earth Planet. Int., **217**, 22–30, doi: 10.1016/j.pepi.2012.11.002.

Šimkanin J., 2016: Hydromagnetic dynamos at the low Ekman and magnetic Prandtl numbers. Contrib. Geophys. Geod., **46**, 3, 221–244, doi: 10.1515/congeo-2016-0 014.

Šimkanin J., Kyselica J., Guba P., 2017: Inertial effects on thermochemically-driven convection and hydromagnetic dynamos in a spherical shell. Geophys. J. Int., doi: 10.1093/gji/ggx529.

Sakuraba A., Roberts P. H., 2009: Generation of a strong magnetic field using uniform heat flux at the surface of the core. Nature Geosci., **2**, 802–805.

Soderlund K. M., Sheyko A., King E. M., Aurnou J. M., 2015: The competition between Lorentz and Coriolis forces in planetary dynamos. Progress in Earth and Planetary Science, **2**, 24, doi: 10.1186/s40645-015-0054-5.

Sreenivasan B., Jones C. A., 2006: Azimuthal winds, convection and dynamo action in the polar regions of planetary cores. Geophys. Astrophys. Fluid Dyn., **100**, 319–339.

Takahashi F., Matsushima M., Honkura Y., 2008: Scale variability in convection-driven MHD dynamos at low Ekman number. Phys. Earth Planet. Int., **167**, 168–178.

Takahashi F., Shimizu H., 2012: A detailed analysis of a dynamo mechanism in a rapidly rotating spherical shell. J. Fluid Mech., **701**, 228–250.

Wicht J., Tilgner A., 2010: Theory and modeling of planetary dynamos. Space Sci. Rev., **152**, 501–542.